Predicting Tumor Location by Modeling the Deformation of the Breast

Article *in* IEEE transactions on bio-medical engineering · November 2008

DOI: 10.1109/TBME.2008.925714 · Source: PubMed

5 authors, including:

Pras Pathmanathan
U.S. Food and Drug Administration
47 PUBLICATIONS **880** CITATIONS
SEE PROFILE

Stephen Chapman
University of Oxford
162 PUBLICATIONS **3,367** CITATIONS
SEE PROFILE

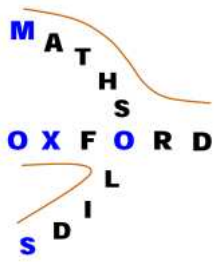

Preprint no. 10/2008

Predicting Tumour Location by Modelling the Deformation of the Breast

P. Pathmanathan, J. Whiteley, S.J. Chapman, D. Gavaghan, and J.M. Brady

Breast cancer is one of the biggest killers in the western world, and early diagnosis is essential for improved prognosis. The shape of the breast varies hugely between the scenarios of magnetic resonance (MR) imaging (patient lies prone, breast hanging down under gravity), X-ray mammography (breast strongly compressed) and ultrasound or biopsy/surgery (patient lies supine), rendering image fusion an extremely difficult task. This paper is concerned with the use of the finite element method and nonlinear elasticity to build a 3D, patient-specific, anatomically-accurate model of the breast. The model is constructed from MR images and can be deformed to simulate breast shape and predict tumour location during mammography or biopsy/surgery. Two extensions of the standard elasticity problem need to be solved: an inverse elasticity problem (arising from the fact that only a deformed, stressed, state is known initially), and the contact problem of modelling compression. The model is used for CC-MLO mammographic image matching, and a number of numerical experiments are performed.

Key words and phrases: breast, deformation, imaging, mechanics

The work reported here forms part of the research programme of OxMOS.

OxMOS: New Frontiers in the Mathematics of Solids
Mathematical Institute
University of Oxford
`http://www2.maths.ox.ac.uk/oxmos/`

April, 2008

Predicting tumour location by modelling the deformation of the breast

Pras Pathmanathan, David J. Gavaghan, Jonathan P. Whiteley, S. Jonathan Chapman, and J. Michael Brady

***Abstract*—Breast cancer is one of the biggest killers in the western world, and early diagnosis is essential for improved prognosis. The shape of the breast varies hugely between the scenarios of magnetic resonance (MR) imaging (patient lies prone, breast hanging down under gravity), X-ray mammography (breast strongly compressed) and ultrasound or biopsy/surgery (patient lies supine), rendering image fusion an extremely difficult task. This paper is concerned with the use of the finite element method and nonlinear elasticity to build a 3D, patient-specific, anatomically-accurate model of the breast. The model is constructed from MR images and can be deformed to simulate breast shape and predict tumour location during mammography or biopsy/surgery. Two extensions of the standard elasticity problem need to be solved: an inverse elasticity problem (arising from the fact that only a deformed, stressed, state is known initially), and the contact problem of modelling compression. The model is used for CC-MLO mammographic image matching, and a number of numerical experiments are performed.**

***Index Terms*—breast, deformation, imaging, mechanics.**

I. Introduction

Breast cancer is one of the biggest killers of women in the western world. Currently, the most common imaging modalities used to image the breast are mammography, magnetic resonance (MR) imaging, and ultrasound. Mammograms (X-rays) are used to obtain projected 2D, high resolution images of the breast. Fig. 1(a) and (b) displays two sample mammograms. MR imaging (see Fig. 1(c)) can be used to produce a set of 2D images of different 'slices' of the breast. However, image-based diagnosis or surgical guidance is severely hindered by the fact that the breast shape varies hugely between these imaging modalities. During MR imaging the patient lies prone, the breasts hanging down under gravity, whereas during surgery or biopsy they lie supine. The change is even more dramatic during mammography, where the breast is tightly compressed in order to spread the tissue. Furthermore, mammograms can be taken from different angles, with two views predominating: cranio-caudal (CC) (compression in the head-to-toe direction) and mediolateral oblique (MLO) (shoulder-to-opposite-hip).

One method of dealing with such issues is to use data from MR images to build a patient-specific anatomically-accurate model of the breast, which can simulate the shape of the breast during surgery or mammography. Such a model would have a wide range of clinical uses. Most importantly, it would allow radiologists to better compare different types of mammogram, or mammograms with MR images. For example, it could be used to predict the curve in (say) an MLO mammogram which corresponds to a point in (say) a CC mammogram, and therefore allow the radiologist to more precisely predict which area in the MLO image corresponds to a suspicious area in the CC image. The model would therefore act as a significant aid to accurate breast cancer diagnosis. By predicting the location of a tumour in the supine position, it could also act as a guide during surgery or biopsy, enabling these procedures to become more reliable, or minimally-invasive. Other applications include use as a visualisation tool, for teaching purposes. Also, an extension of the model could be used simulate the new shape of the breast after reconstructive surgery following a mastectomy (or after cosmetic surgery).

Various methods have been proposed to model breast deformation, mostly based on linear elasticity theory (e.g. [1]), or on non-physical models (e.g. [2]). However, the deformations undergone by the breast can involve large strains, especially during compression, so the full nonlinear theory of elasticity is required. In this paper, we describe the development of a finite element (FE) model of the breast based on nonlinear elasticity theory. A small amount of research (see [3], [4], [5]) has been carried out in the past on MRI-based deformable models of the breast using large strains. Our work differs from these in considering the backward problem (Section II-C) to remove the effect of gravity from the initial state, performing CC-to-MLO image matching, and performing model parameter sensitivity analysis. It differs from [3] in using true nonlinear elasticity theory (a pseudo-nonlinear elastic approach is used in [3]), and not prescribing displacement boundary conditions when modelling compression.

We begin in Section II-A by introducing nonlinear elasticity, and then discuss two re-workings of the standard elasticity problem which we need to consider. The first (Section II-C) is what we term the *backward problem*, which arises because the initial mesh of the breast in a deformed (gravity-loaded) state. Then, in Section II-D, we consider the *contact problem* of modelling compression of the breast for simulating the breast shape during mammography. These different types of problem, and the simulations that are obtained by solving them, are illustrated in Fig. 2. Section III is also a methods section, where we consider image segmentation (Section III-A) and mesh generation (Section III-B). An outline of the image segmentation and mesh generation procedure can be seen in Fig. 3. Results using the model are given in Section IV.

P. Pathmanathan (email pras@comlab.ox.ac.uk), J. Whiteley and D. Gavaghan are with the Oxford University Computing Laboratory, Wolfson Building, Parks Road, Oxford, OX1 3QD, UK.

S. Chapman is with Oxford University Mathematical Institute, 4-29 St Giles, Oxford, OX1 3LB, UK.

J. Brady is with the Oxford University Department of Engineering Science, Parks Road, Oxford, OX1 3PJ, UK.

Manuscript received September 13, 2007.

TABLE I
A SUMMARY OF THE MODELLING ASSUMPTIONS MADE IN THIS WORK, AND REFERENCES TO THE SECTIONS IN WHICH THEY ARE DISCUSSED.

Modelling Assumption	Section discussed in
Zero displacement on the pectoral muscle	II-A
Each individual tissue is homogeneous	III-C
Each individual tissue is isotropic	III-C
All tissues are hyperelastic	(II-A), III-C
All tissues are incompressible	II-A
The breast is not in contact with the breast coils	II-C
Zero friction between skin and compression plates	II-D

First, we simulate deformations of the breast in Section IV-A, and use the compression results to consider the problem of matching a point in a CC mammogram with a curve in an MLO mammogram. Then, in Section IV-B, we use the model to perform a set of numerical experiments, where we investigate the sensitivity of the model to skin, fibroglandular and fatty tissue material parameters, and the effect on the deformation of a tumour modelled as a hard 3D region.

Note that various modelling assumptions are mentioned throughout the paper. These are summarised in Table I, where a reference to the appropriate section is given.

II. Nonlinear Elasticity and the Three Types of Problem

A. Nonlinear Elasticity

Let $\Omega_0 \subset \mathbb{R}^3$ denote an elastic body in its undeformed, unstressed, configuration (the reference state), and let $\Omega \subset \mathbb{R}^3$ be the body in a deformed configuration. Equivalent points in Ω_0 and Ω are denoted $\mathbf{X}$ and $\mathbf{x} \equiv \mathbf{x}(\mathbf{X})$. The deformation gradient is defined to be $F^i_M = \frac{\partial x^i}{\partial X^M}$, from which the right Cauchy-Green deformation tensor $C_{MN} = F^i_M F^i_N$ is defined. The Lagrangian strain is $E = \frac{1}{2}(C - I)$. The Jacobian $J = \det(F)$ is the factor by which volumes transform. $J > 0$ everywhere, and $J = 1$ in the case of incompressibility.

The Cauchy stress tensor [6], denoted σ_{ij}, represents the force measured per unit deformed area acting on the deformed body. The more useful 2nd Piola-Kirchoff stress, T^{MN}, is defined as the force measured per unit undeformed area, acting on a surface in the undeformed body. The two stresses are related by the expression $\sigma = \frac{1}{J} F T F^{\mathrm{T}}$. It can be shown [6] that, for a gravity-loaded object,

$$\frac{\partial \sigma^{ij}}{\partial x^j} + \rho g^i = 0 \qquad \text{in } \Omega, \tag{1}$$

where ρ is the density in the deformed state and $\mathbf{g}$ is gravitational acceleration. The equivalent Lagrangian equation in undeformed space is

$$\frac{\partial}{\partial X^M}\left(T^{MN}\frac{\partial x^i}{\partial X^N}\right) + \rho_0 g^i = 0 \quad \text{in } \Omega_0, \tag{2}$$

where ρ_0 is the density in the reference state. Appropriate boundary conditions are a mixture of prescribed displacements and surface tractions on non-intersecting regions of the boundary. For the breast, our mesh will be created such that the skin is the front surface of the mesh and the pectoral muscle the back surface. We assume zero displacement on the pectoral muscle. This is the simplest assumption to make in the absence of detailed information about the deformation of the muscle for different arm positions. Clearly we should assume zero tractions on the skin surface, and we also assume zero tractions on the remain boundaries of the breast.

Multiplying (1) with a test function $\delta\mathbf{x}$ and integrating by parts, the equivalent weak formulation is easily shown to be

$$\int_\Omega \sigma^{ij}\frac{\partial(\delta x_j)}{\partial x^i}\,\mathrm{d}V - \int_\Omega \rho g^i \delta x_i\,\mathrm{d}V = 0 \qquad \forall\,\delta\mathbf{x}. \tag{3}$$

Similarly, the Lagrangian weak formulation is

$$\int_{\Omega_0} T^{MN}\frac{\partial x^i}{\partial X^M}\frac{\partial(\delta x_i)}{\partial X^N}\,\mathrm{d}V_0 - \int_{\Omega_0}\rho_0 g^i\delta x_i\,\mathrm{d}V_0 = 0 \quad \forall\,\delta\mathbf{x}. \tag{4}$$

Next, we need a relationship between the 2nd Piola-Kirchoff stress to the deformation. We will assume all breast tissues are hyperelastic, which means the stress is a function of strain given by $T^{MN} = \frac{\partial W}{\partial E_{MN}}$, where $W(E_{MN})$ is a material-dependent strain energy function.

We assume all breast tissues are incompressible, since they are composed primarily of water (ignoring the possibility of volume changes due to blood movement when the breast is compressed, due to lack of experimental data), so the incompressibility constraint $\det(F) = 1$ has to be imposed. In this case there is an isotropic internal pressure, denoted p, which contributes to the total stress and is an unknown to be computed. The stress σ then has the form $\sigma^{ij} = \overline{\sigma}^{ij} - p\delta^{ij}$, where $\overline{\sigma}^{ij}$ is the material-dependent part of the stress.

B. The Forward Problem

In the forward problem we assume we know the undeformed shape of the breast and wish to compute the deformed state under applied body forces (i.e. gravity). The four equations which determine the four unknowns $\mathbf{x}$ and p are (2) and the constraint $\det(F) = 1$. The full weak form in this situation is obtaining by summing (4) with the integral of the constraint multiplied by a variation in the pressure, δp, resulting in

$$\begin{aligned} 0 = & \int_{\Omega_0} T^{MN}\frac{\partial x^i}{\partial X^M}\frac{\partial(\delta x_i)}{\partial X^N}\,\mathrm{d}V_0 - \int_{\Omega_0}\rho_0 g^i\delta x_i\,\mathrm{d}V_0 \\ & + \int_{\Omega_0}\delta p(\det F - 1)\,\mathrm{d}V \qquad \forall \delta\mathbf{x}\,,\delta p. \end{aligned} \tag{5}$$

To find the solution of the weak formulation (5), we use the finite element method [7]. Picking a finite set of basis functions to interpolate the unknown deformed position and the unknown pressure, we let $\delta\mathbf{x}$ or δp in (5) be each of these basis functions in turn, in order to obtain a finite set of nonlinear equations. This nonlinear system of equations is solved using Newton's method (with damping) (see [8] for details).

C. The Backward Problem

A mesh generated using MR images of the breast will be of the breast in a deformed, gravity-loaded, state. However, it is assumed in the equations of nonlinear elasticity that the reference state, Ω_0, is unstressed. Before any simulations of surgical or mammographic breast shape can be computed,

we must solve an inverse elasticity problem to obtain the undeformed reference state from the initial mesh, which we call the backward problem[1]. Here, we assume we know the deformed shape and positions, Ω and $\mathbf{x}$, and wish to compute Ω_0 and $\mathbf{X} \equiv \mathbf{X}(\mathbf{x})$. Note that we assume that the breast is not in contact with the breast coils of the MR machine, in any of the MR images, and that the breast hanging freely under gravity, as otherwise we would have to solve a backward contact problem. Note also that, as far as we are aware, no previous work on breast deformation has solved the backward problem when computing breast deformations, even though it is clear from experience that the breast of a post-menopausal woman can be significantly deformed when they are lying in the prone position.

We can compute the solution of the backward problem directly if we begin from (1) or the weak form that is defined on the deformed state (3). Let $G_i^M = \frac{\partial X^M}{\partial x^i} = (F^{-1})_i^M$ be the deformation gradient of the inverse (backward) map. We use G because it is explicitly a function of the known variable $\mathbf{x}$. Incompressibility implies that $\det(G) = 1$. The appropriate weak form for the backward problem is (3), but amended for the incompressibility constraint

$$\begin{aligned} 0 = & \int_\Omega \sigma^{ij}(G,p)\frac{\partial(\delta x_j)}{\partial x^i}\,\mathrm{d}V - \int_\Omega \rho g^i \delta x_i\,\mathrm{d}V \\ & - \int_\Omega (\det(G)-1)\delta p\,\mathrm{d}V \qquad \forall \delta\mathbf{x},\ \delta p \end{aligned} \tag{6}$$

where $\delta\mathbf{x}$ and δp are test functions[2]. This weak form can be solved using the finite element method, using the same techniques as for the forward problem (see [8] for details).

D. The Contact Problem

The contact problem arises when simulating the shape of the breast when compressed for mammography. Contact problems differ from standard forward problems because the region of contact is unknown, and therefore surface tractions, even supposing they were known, cannot be applied as Neumann boundary conditions. The problem has to be formulated an elastic body deforming with the *constraint* that it cannot penetrate the rigid body.

In this paper, we assume frictionless contact between the skin and the compression plates during mammography. Let the gap function, d_N, be defined as the signed normal distance from a point on the skin surface to the nearest point on the compression plates[3]. If d_N is greater than zero it means no penetration of the elastic body into the compression plate has occurred. The total energy equivalent to the weak form (5) is

$$\mathcal{E}(\mathbf{x},p) = \int_{\Omega_0} W\left(E_{MN}\right) - \rho_0 \mathbf{g}\cdot\mathbf{x}\,\mathrm{d}V_0, \tag{7}$$

so the contact problem can be stated as

$$\text{minimise } \mathcal{E}(\mathbf{x},p) \qquad \text{subject to} \quad d_N \geq 0, \tag{8}$$

and also subject to any displacement boundary conditions.

To solve this constrained minimisation problem, we use the Augmented Lagrangian method, where we add an extra term to the total energy, a function of d_N, which penalises violation of the constraints, and then minimise without any constraints (see [8] for more details).

III. Construction of the Model of the Breast

A. Segmentation

To generate a mesh of the breast, we first segment the images to obtain the data needed. Both fibrous and glandular tissue cannot easily be distinguished in MR images, appearing dark gray (see Fig. 1(c)), so we group these tissues together as fibroglandular tissue. Fatty tissue appears light gray. For our purposes we need to complete three tasks: locate the skin boundary, locate the pectoral muscle boundary (which we will take to be the back of the mesh), and segment the interior into fat or fibroglandular tissue (or possibly tumour). The segmentation tasks are illustrated in Fig. 3.

In order to obtain the skin surface, direct thresholding of the background from the breast is suitable for our purposes. Automatic segmentation of the muscle surface is a much more challenging procedure. It is often difficult to manually segment the pectoral muscle in MR images, let alone automate this task. Consequently, methods discussed in the literature for chest wall segmentation of breast-MRI are uncommon and not wholly successful (see, for example [9]). With this is mind, we have resorted to manually segmenting the muscle surface for the data used in this paper. Clearly, this difficulty is one of the major hurdles which needs to be overcome in finite element modelling of the breast. Segmentation of breast MR images is also relatively uncommon, when compared to segmentation of mammograms. We have used a 3D confidence-connected region-growing method [10] to segment the interior.

B. Mesh Generation

For our simulations, we use trilinear basis functions to interpolate position and displacement, with piecewise constant basis functions for interpolating pressure. This forces us to use a hexahedral mesh, as it is well-accepted that tetrahedral elements perform poorly in comparison with hexahedral elements when low-order schemes are used in elasticity problems (see [11] for a discussion). For mesh-generation, a surface-based approach (where a smooth surface is fitted to the boundary of the geometry) was chosen over a voxel-based method (converting voxels or groups of voxels into elements), since smooth surfaces on the mesh boundary are expected to be favourable for contact simulations. Also, we explicitly model

[1]Note that the terminology 'inverse problem' is generally taken to mean the problem of determining material parameters given a deformation. We therefore define the type of problem we wish to solve as a 'backward problem', and call normal elasticity problems 'forward problems'.

[2]Note that the choice of the negative sign before the constraint integral in (6) is very important. Although completely equivalent to using the positive sign, the latter choice would lead to extremely slow GMRES (a method for solving linear systems) convergence. This phenomenon is described further in [8].

[3]i.e. $d_N(\mathbf{x}) = \overline{\mathbf{n}}\cdot(\mathbf{x}-\overline{\mathbf{x}})$, where $\mathbf{x}$ is a point on the skin surface, $\overline{\mathbf{x}}$ the nearest point on the plates, and $\overline{\mathbf{n}}$ the surface normal of the compression plate at $\overline{\mathbf{x}}$. Therefore $d_N = \pm\|\mathbf{x}-\overline{\mathbf{x}}\|$.

the skin as a thin layer of elements, for which the surface-based approach is more appropriate[4].

The mesh generation approach is illustrated in Figures 3 and 4. To construct the geometry of the mesh using a surface-fitting approach, we initially set up a simple rectangular mesh[5], choose cubic-Hermite basis functions to interpolate position, and fit nodal positions and nodal position derivatives to minimise the error between the resultant mesh and the data. Fig. 4(a) displays skin and muscle datapoints which the mesh is to be fitted to (obtained from the segmentation), and the fitted cubic-Hermite mesh is shown in Fig. 4(b). The mesh is converted to a trilinear mesh and refined (Fig. 4(c)), and interior elements are then assigned a tissue type based on the segmentation. The fibroglandular elements are shown in Fig. 4(d). Finally, a layer of thin elements is created on the skin surface and assigned skin material properties. The MR image set was taken of a healthy volunteer and contained no tumour. However, so that we have a reference point with which we can track displacements, we artificially choose a single node on the edge of a fibroglandular element to be a tumour node.

C. Mechanical Properties of Breast Tissue

We have a heterogeneous (three-tissue, excluding tumour) model of the breast, but assume each individual tissue is homogeneous. In reality, fatty tissue in the breast is heterogeneous due to the presence of Cooper's Ligaments, which reinforce the breast in the muscle-to-skin direction. Clearly fibroglandular tissue is not truly homogeneous. There is no consensus in the literature on the anisotropy of healthy breast tissue. In this paper we make the assumption of isotropy for all breast tissues. All tissues are assumed to be hyperelastic, therefore assume that their material laws do not depend on strain rate or history of strain. Most biological tissues display a viscous response to dynamic loading as well as an elastic response. However, since we are looking at static problems and slow loading we assume the forces in the breast are dominated by the elastic response. Also, biological tissues have been shown to have elastic properties that are largely insensitive to strain rate to several orders of magnitude [12]. It is shown in [13] that breast tissues can be modelled primarily as elastic by comparing results of indentation tests at various strain rates.

Suitable experimental data on the mechanical properties of breast tissue is scarce. Most experimental work is restricted to linear elasticity, and are usually confined to *ex vivo* studies. Healthy breast tissue has been shown to be nonlinear [13], with stiffness varying with individual and with age, and in the case of the parenchyma, over the menstrual cycle as well [14]. In general, experimental material laws in the literature for breast tissue are not especially reliable. Precise stress-strain laws proposed for fatty and fibroglandular tissue vary hugely [15]. Even measurements of the Young's modulus of breast tissues can vary by orders of magnitude [16].

There are only a couple of articles in the literature, to the best of our knowledge, which treat breast tissue as hyperelastic. In [17] an incompressible polynomial hyperelastic material law of the form[6]

$$W(I_1,I_2,I_3)=\sum_{0<i+j\leq 2}\alpha_{ij}(I_1-3)^i(I_2-3)^j-\frac{p}{2}(I_3-1) \quad (9)$$

is assumed for breast tissues, where α_{ij} are material parameters that are experimentally estimated (see Table II). We use these laws for fatty and fibroglandular tissue in this work.

TABLE II
EXPERIMENTAL MATERIAL PARAMETERS FOR THE POLYNOMIAL HYPERELASTIC LAW (9) GIVEN IN [17], IN PASCALS.

	α_{10}	α_{01}	α_{20}	α_{02}	α_{11}
Fat	310	300	2250	3800	4720
Fibroglandular	330	280	4490	7720	9450

The mechanical properties of skin have been studied much more extensively than internal breast tissues. Skin has been shown to be anisotropic [18], heterogeneous, nonlinear [19] and visco-elastic [20]. We use an incompressible exponential hyperelastic material law for skin proposed in [19]:

$$W(I_1,I_2,I_3)=a(e^{b(I_1-3)}-1)+c(I_2-3)-\frac{p}{2}(I_3-1), \quad (10)$$

where $a=92.39$Pa, $b=4.4$ and $c=-203.40$Pa.

IV. RESULTS

We now use the model to perform some sample simulations and numerical experiments. A single MR dataset was used for the results in this paper. Ideally these experiments would be repeated on models constructed from a number of different MR datasets on different breasts, but since the model is still in the early stages of its development, and due to the muscle segmentation and mesh generation issues described in Sections III-A and III-B, this is not yet feasible. The MR images were T1-weighted and acquired at Guy's and St. Thomas' Hospital Trust, London, on a 1.5T Philips Gyroscan Intera MR scanner. The image set consisted of 60 slices (with spacing 2.5mm) in the transverse plane, with each slice containing 512 by 512 pixels of size 0.82mm by 0.82mm. Fig. 1(c) shows part of one of the slices. The final mesh constructed from these images, as described in Section III-B, and shown in Fig. 4(d), has 4913 nodes and 4096 elements.

In Section IV-A we use this mesh to first compute the solution to the backward problem, and then the forward and contact problems. For the contact problem we compute the deformation for both CC and MLO compression. The CC and MLO deformations are then used for CC-to-MLO mammographic matching. In Section IV-B we investigate the sensitivity of the model to changes in material parameters for fatty tissue, fibroglandular tissue, and skin. We also look at the effect of including a small hard tumour in the model.

[4]Though not discussed in this paper (see [8] instead), we also wish to model the skin as a membrane, which will entail computing integrals over the skin surface. These integrals use the surface normal, which we wish to be as continuous as possible, forcing the use of a surface-based method.

[5]Note that because we fit a regular mesh of a cuboid to the breast, the final breast mesh contains some badly-shaped elements, and will be less efficient for computation. Development of improved methods of meshing the breast, for example by warping a hemisphere onto the breast rather than a cuboid, is an important task, but was not pursued further for this work.

[6]Here, I_1, I_2 and I_3 are the three principal invariants of C, $I_1=\text{tr}(C)$, $I_2=\frac{1}{2}((\text{tr}(C))^2-\text{tr}(C^2))$ and $I_3=\det(C)$. Isotropic materials have strain energies which are functions only of the principal invariants.

A. Simulations

In this section use the model[7] of the breast to simulate the clinical scenarios discussed in Section I. The first stage is to compute the reference state, by solving the backward problem using the techniques described in Section II-C. This resulted in only a small deformation of the breast formed from the particular MR image set used, with the deformation almost too small for the initial and undeformed meshes to be distinguished visually. The displacement at the nipple node and artificial tumour node were 4.5 and 1.6 mm respectively. Without having clinical data to compare the results with, it is difficult to say whether this magnitude of deformation is realistic or not. On one hand, it is perhaps smaller than would be expected, especially seeing as it appears from Fig. 4(d) that the majority of this breast is fat, and reinforcement due to Cooper's Ligaments has not been modelled. This would possibly suggest that the material parameters in Table II are too large. On the other hand, the initial prone mesh is one which does not appear to have been highly deformed by gravity, which would mean the size of the deformation is as expected. If we then simulate the breast shape during biopsy/surgery by solving the forward problem, the deformation is again a relatively small one. The computation times for the backward and forward problems are 60 minutes and 35 minutes respectively, on a 2Ghz Linux PC[8], demonstrating that simulating deformations of the breast in clinically-viable lengths of time with nonlinear elasticity is computationally tractable.

Next, we simulate mammographic compression, in both the CC and MLO directions. Fig. 5(a) displays the initial mesh with the position of the CC plates. Fig. 5(b) is a view of the CC compressed breast, and Figures 5(c) and 5(d) are two views of the MLO compressed breast. These computations took 114 minutes for the CC simulation and 123 minutes for the MLO simulation. Given the relatively slow machine used, this verifies that compression simulations can also be feasibly solved in clinically acceptable lengths of time.

We can use the compression results to produce simulated CC and MLO mammograms. To do so, in the CC case, we look at all points in the 3D CC compressed breast in the vertical column which would be projected onto a particular pixel, and choose a greyscale value depending on the proportion of fat, fibroglandular tissue and air in that column. Fig. 6(a) is the simulated CC mammogram obtained from the CC compressed breast, and Fig. 6(b) is a simulated MLO mammogram. Note that the simulated MLO image appears more realistic than the CC image only because the view is aligned with the mesh in the CC mammogram, so the edges of the fibroglandular elements are visible (although blurred by the effect of projecting the data onto the image). In the MLO image, the view is at 45 degrees to the element edges, hence the edges are not visible. Also, since the mesh does not include any tissue behind the pectoral muscle, this algorithm is inappropriate for any column of tissue which goes outside the back of the breast. Therefore, the size of the simulated images was chosen so that no pixel corresponded to such columns, hence the pectoral muscle does not appear in the simulated MLO mammogram.

It is not one of our objectives for these simulated mammograms to closely match real mammograms, which would require elements to be of the same size as a mammographic pixel. Instead they are used as the backdrop for the CC-MLO mammographic matching problem, which we can now use the two deformations to solve. The aim is to determine the curve in the MLO image equivalent to a given pixel in the CC image. To do so, we have to sample a number of points in the column in the CC breast corresponding to that pixel, determining for each point the element containing it and the corresponding position in that element. The position of each point in the MLO compressed breast can then be trivially computed using the MLO simulation, and projected onto the MLO mammogram. Fig. 6(a) shows the position of the artificial tumour in the CC mammogram, and Fig. 6(b) shows the curve in the MLO mammogram which maps to that point. For comparison, the curve in the MLO image which is the same distance from the nipple as the tumour is in the CC image is also plotted. This method is sometimes used by radiologists when analysing mammograms from different views; we see that it is very different to the true equivalent curve. Figures 6(c) and (d) display some similar results with a number of different pixels in the CC image.

The resultant curves in the MLO image are surprisingly linear. To investigate this further, let us return to the curve in Fig. 6(b) which corresponds to the tumour pixel. A better idea of the distortion of this line can be found in Fig. 7. Fig. 7(a) displays the CC-compressed breast and the column (which includes the tumour) which is projected onto the tumour pixel. For each point in the column, we can compute the equivalent curve in the reference state, i.e. the uncompressed column. This can be seen in Fig. 7(b), which shows that, although the deformation of the whole breast is very large, the deformation of the column is not very different from simple stretching, especially in the centre of the column. Fig. 7(c) shows the curve in the MLO-compressed breast, where it has been rotated and re-compressed. Again, the compression does not change the shape of the curve a great deal. This is the reason why the final projected curve in Fig. 6(b) is quite close to a straight line.

B. Numerical Experiments

We now use the model to carry out some numerical experiments. Prone-to-supine simulations (a backward simulation followed by a forward one) are more reliable than compression simulations so we use this type of simulation in the experiments[9]. We have chosen the (artificial) tumour and the nipple as two landmarks for which to measure the total displacement.

[7]Note that the deformation code was tested on simplified geometries and for the forward problem by comparing it with independent code, and it was verified that convergence occurs with mesh-refinement. The implementation of the backward problem was tested by solving a forward and then a backward problem on a cube, and verifying the final solution is the original cube.

[8]Note that this is a relatively slow desktop PC.

[9]The displacements are of course significantly smaller in prone-to-supine deformations than CC or MLO deformations, but the model's sensitivity to parameters can still be established by considering the relative and absolute changes in landmark displacement.

TABLE III
PRONE TO SUPINE DISPLACEMENTS (MM) IN SIMULATIONS WITH **VARYING FAT MATERIAL PARAMETERS**. TABULATED ARE: MAGNITUDE OF THE DISPLACEMENT AT THE TUMOUR AND NIPPLE, TOGETHER WITH THE MAGNITUDE OF THESE DISPLACEMENTS RELATIVE TO THE BASE DEFORMATION (THE 100% ROW).

Stiffness	Tumour displacement	Tumour disp. relative to base deformation	Nipple disp.	Nipple disp. relative to base deformation
10%	8.76	5.91	21.04	12.69
50%	4.72	1.72	12.73	4.00
90%	3.26	0.23	9.33	0.55
100%	3.03	0	8.78	0
110%	2.83	0.21	8.26	0.52
200%	1.75	1.29	5.35	3.44
1000%	0.40	2.63	1.29	7.50

TABLE IV
DISPLACEMENTS (MM) IN SIMULATIONS WITH **VARYING FIBROGLANDULAR MATERIAL PARAMETERS**. TABULATED ARE: MAGNITUDE OF THE DISPLACEMENT AT THE TUMOUR AND NIPPLE, TOGETHER WITH THE MAGNITUDE OF THESE DISPLACEMENTS RELATIVE TO THE BASE DEFORMATION (THE 100% ROW).

Stiffness	Tumour displacement	Tumour disp. relative to base deformation	Nipple disp.	Nipple disp. relative to base deformation
10%	3.21	0.30	9.63	0.92
50%	3.12	0.15	9.17	0.42
90%	3.05	0.03	8.85	0.07
100%	3.03	0	8.78	0
110%	3.01	0.03	8.69	0.10
200%	2.86	0.23	8.16	0.66
1000%	2.24	1.02	6.09	2.84

TABLE V
DISPLACEMENTS (MM) IN SIMULATIONS WITH **VARYING SKIN MATERIAL PARAMETERS**. TABULATED ARE: MAGNITUDE OF THE DISPLACEMENT AT THE TUMOUR AND NIPPLE, TOGETHER WITH THE MAGNITUDE OF THESE DISPLACEMENTS RELATIVE TO THE BASE DEFORMATION (THE 100% ROW).

Stiffness	Tumour displacement	Tumour disp. relative to base deformation	Nipple disp.	Nipple disp. relative to base deformation
10%	3.02	0.14	8.96	0.31
50%	3.05	0.03	8.89	0.12
90%	3.03	0.01	8.81	0.03
100%	3.03	0	8.78	0
110%	3.02	0.01	8.76	0.02
200%	2.99	0.04	8.60	0.17
1000%	2.79	0.27	7.76	1.03

Firstly, we consider the sensitivity of the model to material parameters in the interior of the breast. We continue to use 2nd degree polynomial materials laws (9) for fatty and fibroglandular tissue, and study the effect of varying material parameters. We scale each parameter by a constant factor, and want to investigate both small and large changes to the parameters so that either high sensitivity or low sensitivity can be established, and therefore consider $\pm 10\%$ changes to parameters, together with two-fold and ten-fold decreases and increases.

The results of simulations in which the fatty tissue material parameters are rescaled are given in Table III. For these, fibroglandular and skin material parameters are held constant. Tabulated is the magnitude of the prone-to-supine displacement at the landmarks. Since the norm of the displacement at a landmark being close in two simulations does not guarantee the deformations were similar, we also measure the norm of the difference in landmark location between the simulation and the 'base' simulation, which is the simulation with the 'correct' experimental material parameters (i.e. the 100% row in Table III). Table IV displays the equivalent results of simulations where fibroglandular material parameters are varied and fatty tissue parameters are kept constant.

It would be expected that fat plays a much greater role in breast-deformation than fibroglandular tissue, especially for this breast, since the total volume of fat is much higher. The results verify and quantify this. They show it is much more important to have little error in fatty tissue material parameters than fibroglandular material parameters. 10% changes to the total stiffness of fat cause approximately 10% changes to the displacement, but for fibroglandular tissue, a 10% change to stiffness leads to only a 1% change in displacement at both tumour and nipple. The results suggest that much more effort should be expended in determining the mechanical properties of breast fatty tissue *in vivo* than fibroglandular tissue.

Next, we look at the effect of skin on the model. We consider variations in material parameters in the skin material law (10), scaling a and c as they have the dimensions of stiffness, holding b constant. Table V displays the results of varying the skin material parameters. It is clear the stiffness in the skin has very little effect on the deformation, with the only significant changes in the tumour's deformed location coming when the skin stiffness is increased or decreased by a factor of 10. This suggests that the skin, in the form that it is currently modelled, is not a major factor in governing the deformation. However, this conclusion can only be made about the current form of the model, and the results may instead provide an insight into a failing of the model. It is known that human skin is under tension, which we have thus far neglected, since we assume there are no stresses in the reference state. It might be expected that skin plays an important role in the deformation, so the fact that the current model is so insensitive to the skin stiffness could be an indication that this assumption should not have been made. A method of introducing residual stresses in the skin is an open problem, and beyond the scope of this paper. However, this is discussed in [8], where a membrane model of skin is derived, and the backward problem of determining the undeformed shape of a membrane under tension investigated.

We also look at the effect of including a large hard tumour in the finite element model. We hypothesise that a small stiff tumour is unlikely to affect the gross deformation, and investigate this by artificially choosing one whole element to be a tumour element, assigning it the same material law as the fibroglandular elements, and varying its stiffness. The tumour element is obviously larger than a typical tumour detected by screening, but this means that if the model is insensitive to the large artificial tumour we can say it is unlikely to be sensitive to tumours in general. The results given in Table VI show that the model is highly insensitive to tumour stiffness. The tumour has very little impact on the gross deformation (for example, even when the tumour is 20 times stiffer than the

TABLE VI
DISPLACEMENTS (MM) IN SIMULATIONS **WITH ONE TUMOUR ELEMENT, VARYING THE TUMOUR MATERIAL PARAMETERS**. TABULATED ARE: MAGNITUDE OF THE DISPLACEMENT AT THE TUMOUR (LANDMARK) AND NIPPLE, TOGETHER WITH THE MAGNITUDE OF THESE DISPLACEMENTS RELATIVE TO THE BASE DEFORMATION (THE 100% ROW).

Stiffness	Tumour displacement	Tumour disp. relative to base deformation	Nipple disp.	Nipple disp. relative to base deformation
100%	3.03	0	8.78	0
150%	3.02	0.02	8.75	0.04
200%	3.02	0.03	8.76	0.03
500%	3.00	0.08	8.76	0.02
1000%	2.96	0.14	8.74	0.05
2000%	2.92	0.24	8.77	0.02

fibroglandular tissue, the change in the nipple location is just 0.2%), and very little effect on the local deformation. Only when the tumour is 10 times stiffer than the surrounding tissue is there even a 5% change in the tumour location. Tumours are known to be stiffer than healthy breast tissue, but experimental data (e.g. [13]) suggest that they are less than 10 times stiffer. The location of the tumour is possibly a factor in how much it affects the deformation. However, the tumour is not near the fixed chest wall (which is where a tumour would be expected to have the least effect), so we would expect a tumour to have little effect throughout the fibroglandular region. Since such a large tumour does not significantly affect the simulations, the results suggest it is not necessary to include small hard tumours in the models, or at least that their exclusion will not be a major source of error.

Further numerical experiments, including a comparison of the material law (9) with a Neo-Hookean law, and the effect of thin skin on the computation time, are carried out in [8].

V. CONCLUSIONS AND FURTHER WORK

In this paper we have carried out each of the major stages necessary in modelling clinical deformations of the breast, and shown that it is computationally tractable to use nonlinear elasticity to do so. This work was aimed at demonstrating the feasibility and tractability of this approach, rather than developing a fully validated clinically accurate model, which would be the next step. The model is built from MR images, and since MR imaging is less common than mammography or ultrasound, this is a limitation in the clinical applicability of the model. However, a fully-functional accurate model would be a very useful tool when MR images are available, and would possibly encourage the use of MR imaging.

The first task that had to be performed was segmentation of the MR images. Edge-detection of the skin surface was relatively straightforward, but automatic detection of the pectoral muscle surface was a much more difficult task, for which current methods in the literature do not appear totally accurate or robust, and in this work we settled for manual segmentation of the chest wall. This is obviously an unacceptable method for clinical software, and the development of a (semi-)automatic, accurate, robust method of pectoral muscle segmentation (or further investigation into the effect of boundary conditions on the results) is a key task for future work. Using the results in Section IV-B, we can say that it is unlikely to be necessary to include a tumour in a model as a separate 3D sub-region, and therefore automatic methods for segmenting tumours are not critical in this particular line of research. A 3D confidence-connected method was used to segment fatty tissue from the fibroglandular tissue. A comparison of different segmentation methods has not been attempted here, and is left for works dedicated to image analysis. A surface-based method was chosen for mesh-generation method, and another potential area for further work is the development of new algorithms, or application of current algorithms, for producing well-shaped hexahedral meshes of the breast.

The model was then used to simulate prone-to-supine deformations, which were seen to be somewhat smaller than might be expected for a typical post-menopausal woman. It is not clear if this is the correct magnitude of the deformation for this particular dataset, in which case it would be due to the size and geometry of the breast imaged, or if it is due to inaccuracies in the model, such as inaccurate experimental material parameters or features not accounted for. Further experiments need to be done to investigate this, and this is the most important area for further research in this project: the validation of the results using clinical data. We also simulated the breast shape when compressed for both CC and MLO mammography, and used these results to show how it is possible to predict the curve in an MLO mammogram equivalent to a point in a CC mammogram. The results suggested the transformation was dominated by the rotation, rather than the two compressions. We finally performed a number of numerical experiments to study the effect of various factors on the deformations, observing that precision in fat material parameters is more important than in fibroglandular or tumour material parameters. Clinical validation would open up new areas for further numerical experiments. If the simulated deformations do not agree with the experimental results, extensions to the model such as non-zero displacement boundary conditions, a method of modelling blood loss/gain during mammography, frictional contact, or modelling Cooper's Ligaments could be implemented.

ACKNOWLEDGMENT

The authors would like to thank Dr Christine Tanner at University College London for providing the MR data.

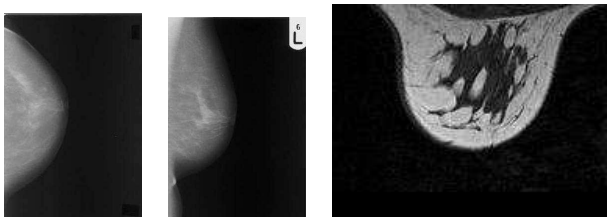

(a) (b) (c)

Fig. 1. (a) A sample CC mammogram, (b) a sample MLO mammogram, (c) part of an MR slice.

REFERENCES

[1] H. Dehghani, M. M. Doyley, B. W. Pogue, S. Jiang, J. Geng, and K. D. Paulsen, "Breast deformation modelling for image reconstruction in near infrared optical tomography," *Phys. Med. Biol.*, vol. 49, pp. 1131–1145, 2004.

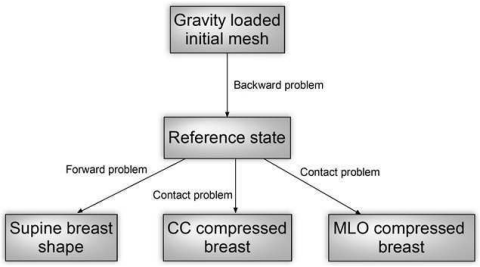

Fig. 2. Schematic of the different types of simulation and the types of problem needed to be solved for each type of simulation.

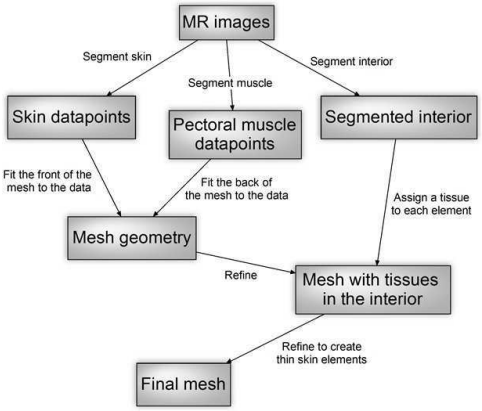

Fig. 3. Schematic of the full mesh-generation procedure. Currently, all stages are semi-automatic except pectoral muscle segmentation, which was done manually.

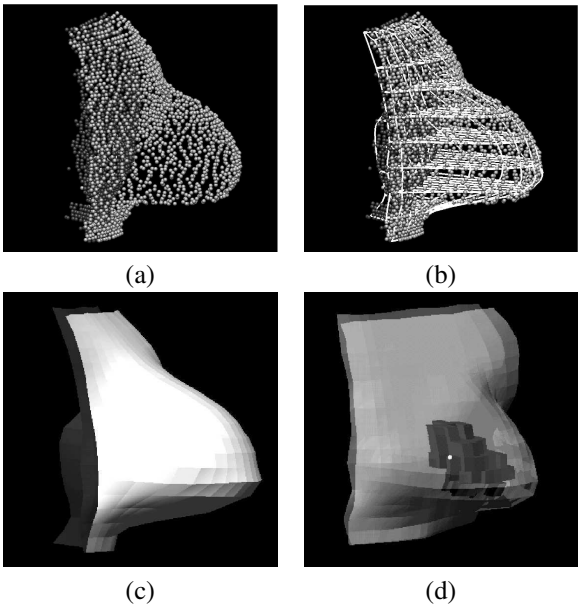

Fig. 4. Mesh generation. (a) Skin (light coloured) and muscle (dark) datapoints (obtained from the segmentation), (b) datapoints and a fitted cubic-Hermite mesh, (c) refined trilinear mesh (only the back surface (dark) and the front surface (light) are shown), (d) refined mesh with translucent front surface so that the fibroglandular elements (dark interior elements) can be seen. The fatty elements are invisible. An artificial tumour is shown as the small bright sphere on the edge of the fibroglandular region.

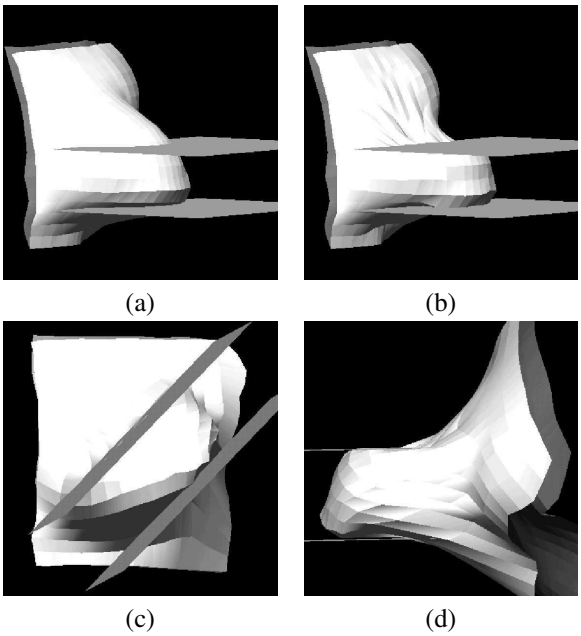

Fig. 5. Simulations of mammographic compression: (a) initial mesh before CC compression, (b) CC compressed breast, (c) MLO compressed breast, (d) alternative view of the MLO compressed breast.

[2] Y. Kita, R. Highnam, and M. Brady, "Correspondence between different view breast X-rays using curved epipolar lines," *Computer Vision and Image Understanding*, vol. 83, no. 1, pp. 38–56, Jul. 2001.

[3] F. Azar, D. Metaxas, and M. Schnall, "A deformable finite element model of the breast for predicting mechanical deformations under external perturbations," *Academic Radiology*, vol. 8(10), pp. 965–975, 2001.

[4] A. Samani, J. Bishop, E. Ramsay, and D. Plewes, "A 3-d contact problem finite element model for breast deformation derived from MRI data," in *Proc. ASB, 23rd Annual Meeting (Pittsburg, PA)*, 1999, p. 72.

[5] D. Plewes, J. Bishop, A. Samani, and J. Sciaretta, "Visualization and quantification of breast cancer biomechanical properties with magnetic resonance elastography," *Physics in Medicine and Biology*, vol. 45, pp. 1591–1610, 2000.

[6] R. Ogden, *Non-linear Elastic Deformations*. Dover Publications, 1997.

[7] J. N. Reddy, *An Introduction to the Finite Element Method*. McGraw-Hill, 1993.

[8] P. Pathmanathan, "Predicting tumour location by simulating the deformation of the breast using nonlinear elasticity and the finite element method," D.Phil Thesis, University of Oxford, 2007.

[9] P. Hayton, "Analysis of contrast-enhanced breast MRI," PhD Thesis, University of Oxford, UK, 1998.

[10] L. Ibanez, W. Schroeder, L. Ng, and J. Cates, *The ITK Software Guide*, http://www.itk.org/ItkSoftwareGuide.pdf.

[11] S. Benzley, E. Perry, K. Merkley, B. Clark, and G. Sjaardema, "A comparison of all-hexahedral and all-tetrahedral finite element meshes for elastic and elasto-plastic analysis," in *Proceedings, 4th International Meshing Roundtable*, 1995, pp. 179–191.

[12] Y. C. Fung, *Biomechanics: Mechanical Properties of Living Tissues*. Springer, 1994.

[13] P. Wellman, R. Howe, E. Dalton, and K. Kern, "Breast tissue stiffness in compression is correlated to histological diagnosis," Harvard Biorobotics Lab., Tech. Rep., 1999.

[14] J. Lorenzen, R. Sinkus, M. Biesterfeldt, and A. Gerhard, "Menstrual-cycle dependence of breast parenchyma elasticity: Estimation with magnetic resonance elastography of breast tissue during the menstrual cycle," *Investigative Radiology*, vol. 38(4), pp. 236–240, 2003.

[15] N. Ruiter, "Registration of X-ray mammograms and MR-volumes of the female breast based on simulated mammographic deformation," PhD Thesis, Universität Mannheim, 2003.

[16] C. Tanner, A. Degenhard, J. A. Schnabel, A. D. C. Smith, C. Hayes, L. I. Sonoda, M. O. Leach, D. R. Hose, D. L. G. Hill, and D. J. Hawkes, "A method for the comparison of biomechanical breast models," in *Proc. IEEE Workshop Mathematical Methods in Biomedical Image Analysis*, 2001, pp. 11–18.

[17] A. Samani and D. Plewes, "A method to measure the hyperelastic

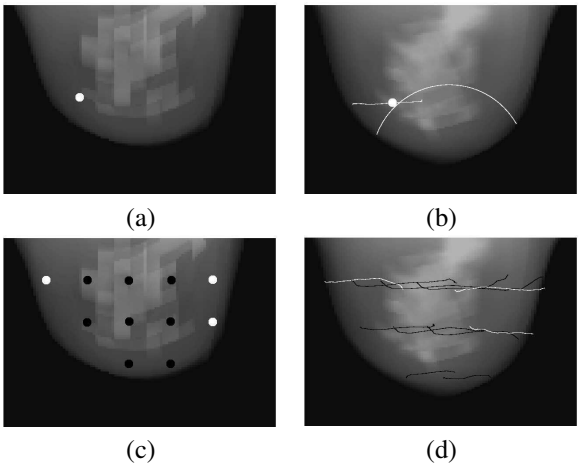

Fig. 6. Simulated mammograms: (a) CC mammogram (with position of tumour shown by a white dot), (b) MLO mammogram (with computed line corresponding the CC tumour point (shorter line), actual position of tumour (dot), and a guess according to distance from nipple (longer arc of circle)), (c) CC mammogram with a selection of points, (d) MLO mammogram with equivalent curves to the points in (c). Note that the MLO image does not go far back enough to see the pectoral muscle.

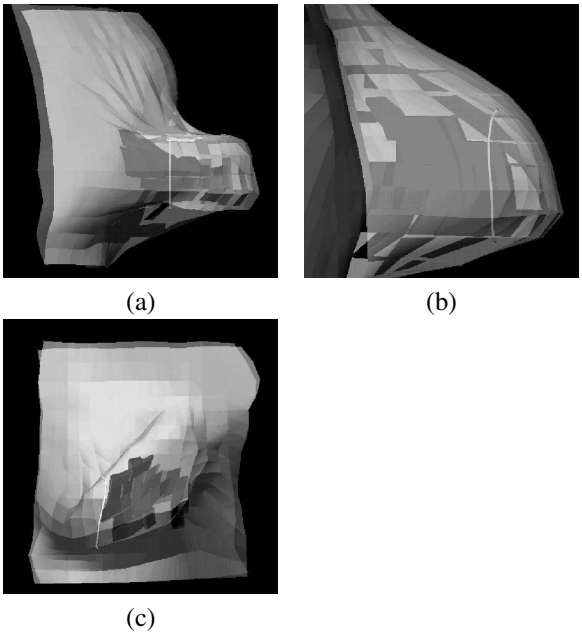

Fig. 7. CC to MLO matching. In all figures the muscle is the dark back surface, the fibroglandular region are the dark interior elements, and the skin is the translucent light surface. The light line represents: (a) the line which is projected onto the tumour pixel in the CC breast, (b) the equivalent uncompressed line in the reference state, (c) the equivalent line in the MLO compressed breast.

parameters of *ex vivo* breast tissue samples," *Physics in Medicine and Biology*, vol. 49, pp. 4395–4405, 2004.

[18] Y. Fung, "Biomechanics: Its scope, history, and some problems of continuum mechanics in physiology," *Applied Mechanics Reviews*, vol. 21(1), pp. 1–20, 1968.

[19] D. R. Veronda, "Mechanical characterization of skin-finite deformation," *Journal of Biomechanics*, vol. 3, pp. 111–124, 1970.

[20] P. Agache, C. Monneur, J. Leveque, and J. de Rigal, "Mechanical properties and Young's modulus of human skin *in vivo*," *Archives of dermatological research*, vol. 269(3), pp. 221–32, 1980.